J. Phys. D: Appl. Phys. **30** (1997) 3071–3078. Printed in the UK PII: S0022-3727(97)84231-3

The multiphoton photo-effect and harmonic generation at metal surfaces

S Varró† and F Ehlotzky‡

† Research Institute for Solid State Physics of the Hungarian Academy of Sciences, PO Box 49, H-1525 Budapest, Hungary
‡ Institute for Theoretical Physics, University of Innsbruck, Technikerstraße 25, A-6020 Innsbruck, Austria

Received 16 May 1997, in final form 29 July 1997

Abstract. By using a dipole-layer model for the scattering of electrons at a metal surface in a laser field, we show that, at relatively moderate laser intensities of some 10^{10} W cm^{-2} of a Nd:YAG laser, photo-electrons of very high nonlinear order are generated having energies of up to about 500 eV. Similarly, we predict harmonics of very high order under the same parameter conditions. The high-order electron-energy spectrum agrees very well with recent observations by Farkas *et al* (*Phys. Rev.* A **41** 4123 (1990); *Opt. Eng.* **32** 2476 (1993)). With our model predictions one does not need to resort to the mechanism of Coulomb explosion in order to explain the observed high-energy photo-electrons.

1. Introduction

With increasing power of the available laser sources the investigation of the multiphoton ionization and harmonic generation brought about by shining laser light onto atoms became a subject of very active research [1, 2]. Similarly, it has become of interest to consider these processes at metals since the density of active electrons at solid surfaces is very high. When one is investigating the multiphoton photo-effect and harmonic generation at metal surfaces, one has to distinguish between two different regimes. If the laser power is very high and the laser pulses are very short, then a radiation-compressed surface plasma gets formed and harmonics can be formed in this over-dense quasi-free-electron cloud [3–6]. In the second case, which will be considered here, much effort is devoted to keeping the solid surface unheated. This requires the use of a rather low laser power of some 10^9–10^{10} W cm^{-2} and picosecond laser pulses. Such experiments have been performed more recently by Farkas and co-workers [7–9]. In these experiments rather high-energy photo-electrons were observed which had not been predicted by the existing model calculations [10–12]. It has been argued that the observed high-energy electrons of a few hundred electron-volts may have their origin in Coulomb explosion [13] but very recent experiments by Farkas *et al* [9] showed that this mechanism cannot explain the discreteness of the observed photo-electron spectrum.

It is the purpose of the present paper to suggest a model which explains the occurrence of high-energy photo-electrons and predicts simultaneously the generation of harmonics at very high nonlinear order. Our model is based on a remark by Liebsch and Schaich [14] that, for generation of harmonics at solid surfaces, polarization effects play a crucial role. We therefore present in the following a simple model calculation which is based on the formation of a surface dipole layer induced by the presence of the laser field and we consider the scattering of a test charge of the solid by this dipole field oscillating in time with the period of the laser radiation.

2. The dipole model of the multiphoton photo-effect

We consider a laser beam which is impinging under grazing incidence on a metal surface such that the laser polarization is almost perpendicular to the surface. This field will induce at the surface in each pair of ion core and associated electrons an oscillating dipole moment directed perpendicularly to the solid surface. If we sum up the contributions of all these dipoles along the surface of the solid, they will yield a dipole-layer potential for a test charge $-e$ near the surface and this dipole-layer potential will oscillate with the laser frequency. The general idea behind these assumptions is the following. In a monovalent metal like gold, used in the experiments of Farkas and co-workers [7–9], at any instant of time we may associate with every Wigner–Seitz cell around an ion near the surface on the average one quasi-free conduction electron. The gas of quasi-free electrons, however, is subjected to density fluctuations so that there will always be electrons near the surface of the solid which have no ion as their partner. These will be those electrons which

have come under the influence of the above laser-induced dipole potential and which will become the ionized photoelectrons. This ionization process has formally to be treated within the framework of quantum-mechanical scattering theory whereby the wavefunction of the ionizing electron under the influence of the above dipole-layer potential as well as the static potential of the metal have to be matched at the boundary between the interior and exterior regions near the metal surface. Of course, since the density of electrons in the metal is so large, in the case of gold 5.9×10^{22} cm^{-3}, we may safely neglect the depletion of electrons near the surface of the solid due to ionization. Consequently, it is a reasonable assumption to have on the one hand electron–ion pairs near the surface yielding dipole oscillations in the laser field and, on the other hand, electrons on which the generated dipole forces are acting. This is the basis of our considerations below.

In figure 1 $\boldsymbol{\xi}(t)$ is the laser-induced displacement of an electron near the surface with respect to the corresponding ion core which is considered at rest. The potential energy stemming from an ion at position $\boldsymbol{r}_j$ and the corresponding electron at position $\boldsymbol{r}_j + \boldsymbol{\xi}(t)$ for a test charge $-e$ is then given by

$$V_j = \frac{e^2}{|\boldsymbol{r} - (\boldsymbol{r}_j + \boldsymbol{\xi})|} - \frac{e^2}{|\boldsymbol{r} - \boldsymbol{r}_j|} \cong e^2 \frac{\boldsymbol{\xi} \cdot (\boldsymbol{r} - \boldsymbol{r}_j)}{|\boldsymbol{r} - \boldsymbol{r}_j|^3} + \cdots \quad (1)$$

where we have made an expansion of V_j up to first order in $\boldsymbol{\xi}(t)$. Now we sum up all the contributions of the V_j terms by going over to the continuum limit. This yields

$$V = \sum_j V_j \to e^2 n_e \int \mathrm{d}x' \, \mathrm{d}y' \, \mathrm{d}z' \times \frac{\xi_z(t)(z - z')}{[(x - x')^2 + (y - y')^2 + (z - z')^2]^{3/2}} \quad (2)$$

where we have introduced the electron density n_e which is assumed to be the same as the ion density because of the charge neutrality of the solid. In the numerator of (2) the x and y components of $\boldsymbol{\xi}(t)$ do not show up since they drop out due to the axial symmetry of the problem with respect to the z axis perpendicular to the metal surface (see figure 1). On going over to polar coordinates $x' - x = \rho \cos\varphi$, $y' - y = \rho \sin\varphi$ and performing the integrations with respect to ρ and φ, we get for the dipole potential V

$$V = 2\pi n_e e^2 \int_{-\infty}^{0} \mathrm{d}z' \xi(z', t) \frac{z - z'}{|z - z'|} \quad (3)$$

where $(z - z')/|z - z'| = 1$ for $z > z'$ and -1 for $z < z'$. In order to evaluate the integral in (3), we have to know the functional form of $\xi(z', t)$. Let us assume that the distribution of $\xi(z', t)$, stemming from the laser field of electric field strength F_0 inside the solid is given by

$$F = F_0 \exp(z'/\delta) \sin(\omega t) \quad (4)$$

where ω is the laser frequency and δ the skin depth in the metal. By solving Newton's equation of motion for the electron in the presence of the above field we get

$$\xi(z', t) = \alpha_0 \exp(z'/\delta) \sin(\omega t) \qquad \alpha_0 = eF_0/(m\omega^2). \quad (5)$$

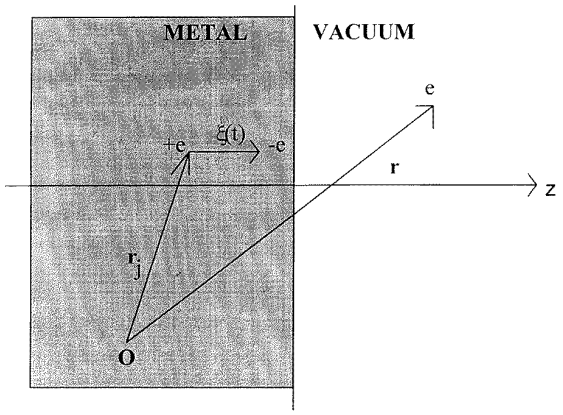

Figure 1. The relative positions of an ion core, of its associated electron and of the test charge near the solid surface.

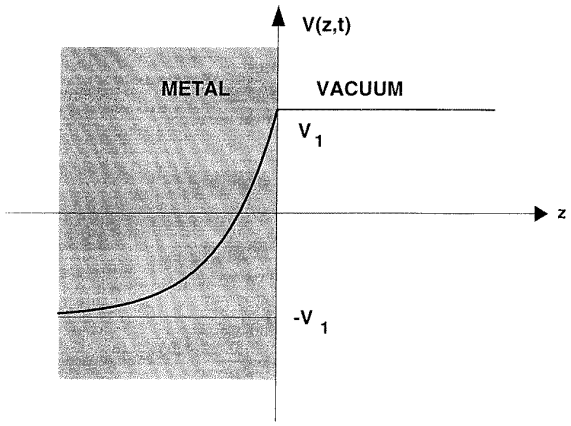

Figure 2. The oscillating dipole layer at the phase $\omega t = \pi/2$.

On introducing this into (3) by observing the special property of the argument of (3) we find for $z > 0$

$$V = 2\pi n_e e^2 \delta \alpha_0 \sin(\omega t) \quad (6a)$$

and for $z < 0$

$$V = 2\pi n_e e^2 \delta [2 \exp(z/\delta) - 1] \alpha_0 \sin(\omega t). \quad (6b)$$

For a certain instant of time, say $\omega t = \pi/2$, the potential given by (6a) and (6b) is shown schematically in figure 2. In figure 2 we have introduced the abbreviation V_1 which is the amplitude of the oscillating double-layer potential and which is given by

$$V_1 = 2\pi n_e e^2 \delta \alpha_0 = \tfrac{1}{2}(\omega_p/\omega)^2 (\delta/\lambda\!\!\!^{-}) \mu m c^2 \quad (7)$$

where we used the definition of the plasma frequency $\omega_p^2 = 4\pi n_e e^2/m$.

$\lambda\!\!\!^{-} = \lambda/(2\pi) = c/\omega$ is the inverse of the wavenumber of the laser field. Moreover, we have defined the widely used dimensionless intensity parameter μ which can be expressed in the form

$$\mu = eF_0/(mc\omega) = 10^{-9} I^{1/2}/E_{ph} \quad (8)$$

where the laser intensity I is measured in W cm^{-2} and E_{ph} measures the photon energy in electron-volts. In general, the skin depth δ is given by the expression

$$\delta = c/(\omega_p^2 - \omega^2)^{1/2} \cong c/\omega_p \tag{9}$$

in which the last approximation is accurate as long as $\omega_p \gg \omega$. This is the case for the experiments mentioned in the introduction in which the target metal was gold for which $\hbar\omega_p = 10.53$ eV whereas the photon energy of the used Nd:YAG laser is $\hbar\omega = 1.17$ eV. In the above approximation, V_1 of (7) can be written as

$$V_1 = \tfrac{1}{2}(\omega_p/\omega)\mu mc^2. \tag{7a}$$

In order to get a feeling for the size of V_1, as given by the approximation (7*a*), we evaluated it for gold at a laser intensity of 2.5×10^{10} W cm^{-2}. In this case we have $\omega_p/\omega = 9$ and $\mu = 1.35 \times 10^{-4}$. With these parameter values V_1 turns out to be 304 eV.

Before we continue, let us consider the fact that, classically, an electron near the surface of the metal can radiate under the action of the above dipole potential. Starting from (6*b*) we get from Newton's equation of motion

$$\mathrm{d}_t p_z = -\partial_z V(z=0) = -4\pi n_e e^2 \alpha_0 \sin(\omega t)$$

$$\mathrm{d}_{tt} z = -(4\pi n_e e^2 \alpha_0/m)\sin(\omega t) \tag{10}$$

and hence we find from Larmor's formula for the radiated power or, more conveniently, for the scattering cross section

$$\begin{aligned}\mathrm{d}\sigma/\mathrm{d}\Omega &= [e^2/(4\pi c^3 I)]\langle(d_{tt}z)^2\rangle \sin^2\theta \\ &= (r_0/\pi)^2 (r_0 \lambda^2 n_e)^2 \sin^2\theta\end{aligned} \tag{11}$$

where I is the laser intensity, θ is the angle of radiation emission with respect to the laser polarization perpendicular to the surface of the metal and r_0 is the classical electron radius. The angle brackets indicate averaging over one laser period. Since for the Nd:YAG laser used in the experiments $\lambda = 1064$ nm, $n_e = 5.9 \times 10^{22}$ cm^{-3} and $r_0 = 2.8 \times 10^{-13}$ cm we find $\mathrm{d}\sigma/\mathrm{d}\Omega = 16.8 r_0^2 \sin^2\theta$ which is only slightly larger than the Thomson cross section. So far one would think that classically there is no harmonic generation. This, however, we obtain by properly taking into account the laser-induced retardation effects which are caused by the large amplitude of electron oscillation in the laser field. As we showed many years ago [15], the correctly retarded acceleration can be written to first order of approximation in the following form:

$$\mathrm{d}_{\tau\tau} z(\tau) = -(4\pi n_e e^2 \alpha_0/m)\sin\{\omega[\tau - (z(\tau)/c)\cos\theta]\} \tag{12}$$

where $\tau = t - r/c$ is the average retarded time. By performing in (10) the two time integrations to get $z(\tau)$, we find after insertion of $z(\tau)$ into (12) and Fourier decomposition the following nonlinear cross sections for the nth order harmonics as the corresponding generalization of (11):

$$\begin{aligned}\mathrm{d}\sigma_n/\mathrm{d}\Omega &= 16.8 r_0^2 \sin^2\theta J_n^2(a_{cl}) \\ a_{cl} &= [\alpha n_e \lambda_c \lambda^2 \mu/(2\pi^2)]\cos\theta\end{aligned} \tag{13}$$

where J_n is an ordinary Bessel function of order $n \geq 0$ and a_{cl} is a classical parameter to be compared later on with the parameter a of our quantum mechanical calculations. In a_{cl}, α is the fine-structure constant, λ_c the Compton wavelength and μ the intensity parameter introduced in (8). Using the corresponding parameter values of the laser and the target and taking $I = 10^{10}$ W cm^{-2}, we get for the maximum value of $a_{cl} = 5.3 \times 10^{-3} \ll 1$ and hence the harmonic efficiency is negligibly small.

After this excursion into the classical domain, assuming that the generation of harmonics at metal surfaces can be treated classically, we return to our quantum-mechanical treatment. In fact, since the photo-effect and its generalization, the multiphoton photo-effect, are quantum mechanical-processes, their accompanying process of harmonic generation also has to be treated quantum mechanically and this will yield results entirely different from those of our foregoing classical analysis.

Going back to equations (6*a*) and (6*b*), we shall in the following simplify our analysis of electron scattering at the solid surface in the presence of the above dipole-layer potential. We shall approximate this potential, which is depicted in figure 2, by an oscillating potential step by taking for the amplitude of V at $z < 0$ its asymptotic value $-V_1$ for $z \to -\infty$. Hence we use an idealized double-layer potential which oscillates with the frequency of the laser field between the two extreme values $-V_1$ and $+V_1$ in opposite phase for $z < 0$ and $z > 0$. The static potential exerted by the metal surface on the test electron will be described in the spirit of the Sommerfeld model of a metal by the step function $V_0(z) = V_0[\Theta(z) - 1]$, where $\Theta(z)$ is Heaviside's step function and V_0 is the depth of the potential well.

In this way the relevant Schrödinger equations, governing the scattering process in the two regions $z < 0$ and $z > 0$ can be written in the form

$$[\hat{p}^2/(2m) - V_0 - V_1 \sin(\omega t)]\Psi_I = \mathrm{i}\hbar\partial_t \Psi_I \qquad (z < 0) \tag{14a}$$

$$[\hat{p}^2/(2m) + V_1 \sin(\omega t)]\Psi_{II} = \mathrm{i}\hbar\partial_t \Psi_{II} \qquad (z > 0). \tag{14b}$$

In order to satisfy the boundary conditions at $z = 0$, we have to make a Floquet Ansatz in both regions in terms of the fundamental solutions of the above equations. Thus we put

$$\begin{aligned}\Psi_I = &\left(\chi_0^{(+)} - \chi_0^{(-)} + \sum_n R_n \chi_n^{(-)}\right) \\ &\times \exp\{-\mathrm{i}[V_1/(\hbar\omega)]\cos(\omega t)\}\end{aligned} \tag{15a}$$

$$\Psi_{II} = \sum_n T_n \varphi_n^{(+)} \exp\{+\mathrm{i}[V_1/(\hbar\omega)]\cos(\omega t)\} \tag{15b}$$

where

$$\begin{aligned}\chi_0^{(\pm)} &= \exp(\pm \mathrm{i} q_0 z/\hbar - \mathrm{i} E_0 t/\hbar) \\ \chi_n^{(-)} &= \exp[-\mathrm{i} q_n z/\hbar - \mathrm{i}(E_0 + n\hbar\omega)t/\hbar]\end{aligned} \tag{16}$$

with the momenta q_n satisfying the free-mass-shell relations

$$q_n = [2m(V_0 + E_0 + n\hbar\omega)]^{1/2}. \tag{16a}$$

Similarly,

$$\varphi_n^{(+)} = \exp[+\mathrm{i} p_n z/\hbar - \mathrm{i}(E_0 + n\hbar\omega)t/\hbar]$$

$$p_n = +[2m(E_0 + n\hbar\omega)]^{1/2}. \tag{17}$$

The unknown reflection coefficients R_n and transmission coefficients T_n can be determined from the matching equations, the first of which is

$$\Psi_I(0,t) = \Psi_{II}(0,t) \tag{18}$$

from which follows that, for all values of t, the following relations hold:

$$R_n = \sum_k J_{n-k}(a)\mathrm{i}^{n-k}T_k. \tag{18a}$$

These relations are obtained by applying to (18) in its explicit form the Fourier-expansion theorem with respect to t using the Jacobi–Anger formula which is generating the ordinary Bessel functions J_n of order n. The parameter a appearing in (18a) as the argument of the Bessel functions is defined by

$$a = 2V_1/(\hbar\omega). \tag{19}$$

It represents the maximum amplitude of the oscillating dipole layer expressed in units of the photon energy and should be compared with our above classical parameter a_{cl} as given by (13). Whereas V_1 of (7a) represents a classical expression, the parameter a of (19) is apparently of quantum-mechanical origin and we therefore expect results from our quantum-mechanical calculations entirely different from those from our foregoing classical considerations, though in both cases the results can be expressed by Bessel functions. Similarly, we get from the continuity condition for the derivatives of the wavefunctions

$$\partial_z\Psi_I(0,t) = \partial_z\Psi_{II}(0,t) \tag{20}$$

the relations

$$2q_0\delta_{n,0} - q_nR_n = \sum_k J_{n-k}(a)\mathrm{i}^{n-k}p_kT_k \tag{20a}$$

where the Bessel functions have the same argument (19) as before. By combining (18a) and (20a) one can derive a closed infinite set of linear algebraic equations for the transmission coefficients T_k

$$\delta_{n,0} = \sum_k J_{n-k}(a)\mathrm{i}^{n-k}\frac{q_n + p_k}{2q_0}T_k. \tag{21}$$

Once we know the solution of (21) for the transmission coefficients T_n, then, on account of (20a), we also know the reflection coefficients R_n. The time-averaged outgoing current components (for which the momenta p_n are real) corresponding to the absorption or emission of $|n|$ photons, can be obtained from Ψ_{II} of (15b) by using the standard formula of quantum mechanics yielding the probability current density. For convenience we normalize these current components with respect to the incoming current density in order to get dimensionless quantities. So we define the normalized components of the transmitted current density by

$$j_t(n) = (p_n/q_0)|T_n|^2 \tag{22}$$

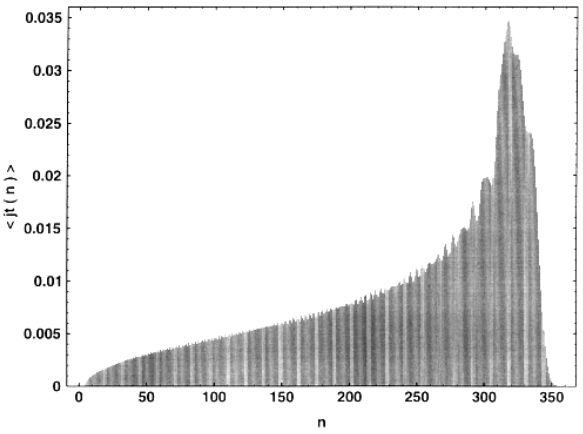

Figure 3. The intensity-averaged transmitted probability currents $j_t(n)$ in the Born approximation as a function of n for a laser intensity of 10^{10} W cm^{-2} (a = 330).

which is valid for $n \geq n_0$, where n_0 is the minimum number of photons to be absorbed in order to have true free-running outgoing waves. If $n < n_0$ then the components (17) associated with such momenta are evanescent waves bound to the surface of the metal. In a similar fashion we define the normalized components of the reflected current by

$$j_r(n) = (q_n/q_0)|R_n - \delta_{n,0}|^2 \tag{23}$$

this being valid for $n \geq n_1$, where n_1 has a similar meaning to that of n_0 before. The conservation of probability condition requires that the sum of the normalized reflected and transmitted current components be unity; that is

$$\sum_{n=n_1}^{\infty} j_r(n) + \sum_{n=n_0}^{\infty} j_t(n) = 1. \tag{24}$$

This condition can serve as a check for testing the accuracy of the numerical solutions of the matching equations (18a), (20a) and (21).

Unfortunately, (21) cannot be solved analytically. If we truncate this set of equations in order to get a numerical solution, the accuracy of this approximate solution will of course depend on the size of the truncated kernel matrix. On the other hand, it is intuitively clear that the size of the truncated kernel matrix to be taken crucially depends on the value of the parameter a given by (19). For instance, for the example of $V_1 = 304$ eV, mentioned previously, we find $a = 250$ (which is six orders of magnitude larger than a_{cl}). In this case an accurate result can certainly not be obtained with a truncated kernel matrix of a size less than 1000×1000.

Fortunately, for very large values of the parameter a the solutions T_n of (21) can be well approximated by an analytical formula, at least for large values of n. In order to find this analytical approximation, we proceed as follows. First we write down an alternative form of (21):

$$\delta_{n,0} = \sum_k J_{n-k}(a)\frac{q_n + p_k}{2q_0}T_k\mathrm{i}^{-k}. \tag{25a}$$

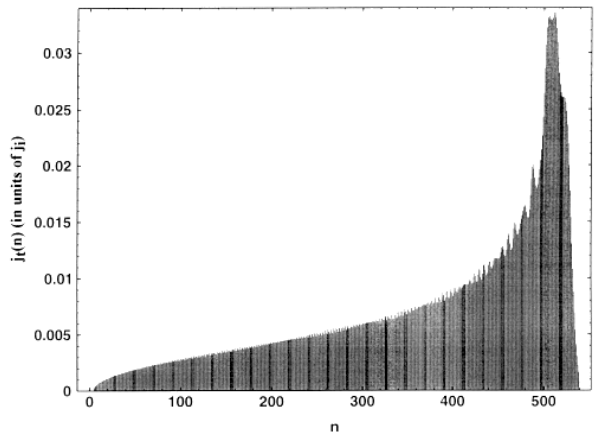

Figure 4. Similar data to those in figure 3 for an intensity of 2.5×10^{10} W cm^{-2} ($a = 520$).

and multiply this equation by $J_{s-n}(-a)$ and take the sum over n. Thus we get after the index transformation $n-k = \ell$

$$J_s(-a) = \sum_{k,\ell} J_{s-k-\ell}(-a) J_\ell(a) \frac{q_{\ell+k} + p_k}{2q_0} T_k \mathrm{i}^{-k}. \quad (25b)$$

If we now approximate $(q_{\ell+k} + p_k)/(2q_0)$ by unity, then the summation in (25b) over ℓ can be carried out exactly on account of the addition theorem of Bessel functions yielding $J_{s-k}(-a+a) = \delta_{s,k}$. Hence we get in this approximation for the transmission coefficients

$$T_n \cong J_n(-a)\mathrm{i}^n \quad (25c)$$

and therefore for the transmitted currents the approximation

$$j_t(n) \cong (p_n/q_0) J_n^2(a). \quad (25d)$$

At the same time we get from (18a), by inserting (25c) and employing the addition theorem of Bessel functions, $R_n = \delta_{n,0}$ and hence there are no reflected currents (23). In spite of this, the transmitted currents do not satisfy the sum rule

$$\sum_{n=n_0}^{\infty} j_t(n) = 1$$

since for small values of n the above approximation involving (25c) and (25d) is certainly very crude. This approximation relies essentially on the assumption that the average energy of the emitted electron is much larger than the energy of a single photon and also much larger than the binding energy V_0. Mathematically this corresponds to approximating the transformed kernel in (25b) by a unit matrix. We shall call this approximation the Born approximation, which will be justified and become clear in the following when we consider our process from the point of view of scattering theory.

Let us take an incoming wave solution of the Schrödinger equation (14a) as an initial state

$$\Psi_{q_0} = L^{1/2} \exp[\mathrm{i}q_0 z/\bar{h} - \mathrm{i}E_0 t/\bar{h} - \mathrm{i}(a/2)\cos(\omega t)] \quad (26a)$$

and an outgoing final state as a solution of (14b)

$$\Psi_p = L^{1/2} \exp[\mathrm{i}pz/\bar{h} - \mathrm{i}Et/\bar{h} + \mathrm{i}(a/2)\cos(\omega t)]. \quad (26b)$$

The first-order Born amplitude for scattering from the initial state (26a) to the final state (26b) due to the interaction with the static Sommerfeld potential $V_0(z) = V_0[\Theta(z) - 1]$ is then given by

$$T_{fi} = -(\mathrm{i}/\bar{h}) \int \mathrm{d}t \langle \Psi_p | V_0(\hat{z}) | \Psi_{q_0} \rangle. \quad (26c)$$

The integration over time can be easily carried out by Fourier decomposing the integrand by means of the Jacobi–Anger formula used previously. Thus we obtain an incoherent sum of partial amplitudes corresponding to $|n|$-photon emission or absorption, namely

$$T_{fi} = \sum_n T_{fi}^{(n)}$$

$$T_{fi}^{(n)} = -2\pi \mathrm{i}\delta(E - E_0 - n\bar{h}\omega) t_{fi}^{(n)} \quad (27a)$$

with

$$t_{fi}^{(n)} = L^{-1} V_0(q_0 - p) J_n(-a)\mathrm{i}^n \quad (27b)$$

where

$$V_0(q_0 - p) = \int \mathrm{d}z\, V_0(z) \exp[\mathrm{i}(q_0 - p)z/\bar{h}] \quad (27c)$$

is the Fourier transform of the Sommerfeld potential. On introducing the explicit form of $V_0(z)$ we find $V_0(q_0 - p) = V_0\bar{h}/(q_0 - p)$. The Dirac delta function in (27a) expresses the energy balance during the process. By using the free-mass-shell relations (16a) and (17) for q_0 and p respectively, we obtain $V_0/(q_0 - p) = (q_0 + p_n)/(2m) \geq p_n/m$. By employing now the standard procedures to get from (27b) and (27c) the transition probabilities per unit time we find for an nth-order process

$$W_n = [p_n/(mL)] J_n^2(a). \quad (28)$$

This relation represents the flux components of the outgoing electrons. By normalizing these with respect to the incoming flux we recover exactly the approximation (25d).

For the following numerical examples we have chosen gold as the target material since it was used in the experiments by Farkas and co-workers [7–9]. In this case we have the following input parameters: the depth of the Sommerfeld potential $V_0 = 10.19$ eV, the Fermi energy $E_F = 5.$ eV, the work function $A = 4.68$ eV and $\bar{h}\omega_p = 10.53$ eV. As the laser source we took a Nd:YAG laser with photon energy $\bar{h}\omega = 1.17$ eV.

In figure 3 we show the transmitted current-density distribution $j_t(n)$ of the emitted electrons as a function of the number of absorbed photons. The data presented were obtained by averaging over a small intensity range in order to take into account the laser fluctuations of realistic radiation sources. The currents were evaluated for a laser intensity of $I = 10^{10}$ W cm^{-2} and the Born approximation (25d), discussed above, was employed since the characteristic parameter a (19) has in this case the value $a = 330$ in which case the matrix inversion in (25a) becomes prohibitively computer-time consuming.

We show in figure 4 similar data for an intensity of $I = 2.5 \times 10^{10}$ W cm^{-2} in which case the parameter $a = 520$. As we can see, in both cases our model predicts

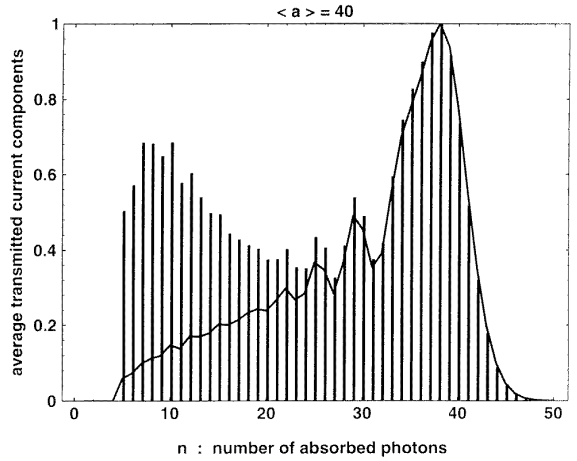

Figure 5. A comparison of the transmitted currents (bars) obtained from solving (21) and (22) and (full line) by using (25*d*), for $a = 40$.

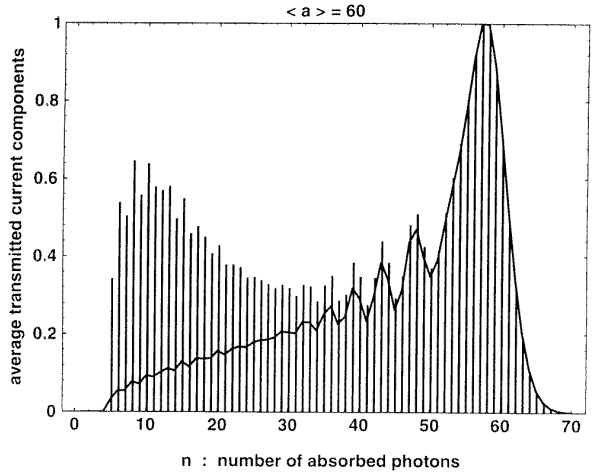

Figure 6. Similar data to those in figure 5 but for $a = 60$.

energies of the photo-electrons of up to a few hundred electron-volts, in agreement with the experiments [7, 8].

In order to demonstrate the accuracy of our Born approximation (25*d*) for the emitted electrons at high nonlinear order n, we show in figure 5 the transmitted currents $j_t(n)$ obtained on the one hand from performing the matrix inversion of (25*a*) and, on the other hand, by using the approximation (25*d*). In figure 5 the parameter a was taken equal to 40, in which case the matrix inversion could still be accomplished during a reasonable amount of computer time. As one can see, at high orders n, starting at about $n = 25$, the agreement between the exact data, represented by bars, and the approximate data, drawn as a full line, is surprisingly good. Similar values are shown in figure 6, in which $a = 60$, in which case the agreement between the data from matrix inversion and the Born approximation starts at about $n = 35$.

Since the integrated transmitted currents were observed experimentally by Farkas and Tóth [7, 8], we show these currents in figure 7 for three different values of the intensity.

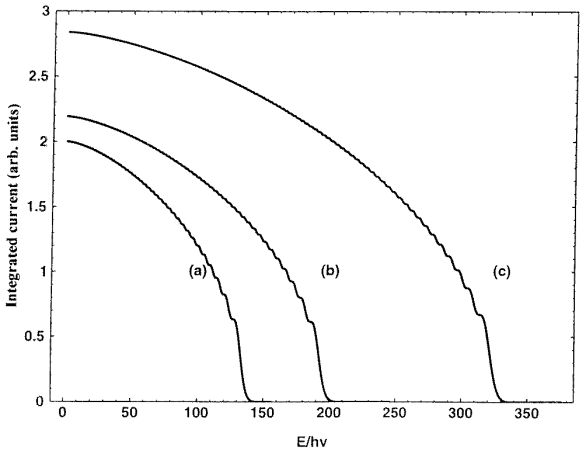

Figure 7. The integrated currents, as explained in the text, for (a) $I = 3.1 \times 10^9$ W cm^{-2} ($a = 140$), (b) $I = 3.7 \times 10^9$ W cm^{-2} ($a = 200$) and (c) $I = 10^{10}$ W cm^{-2} ($a = 330$).

Curve (a) corresponds to $I = 3.1 \times 10^9$ W cm^{-2} ($a = 140$), curve (b) to $I = 3.7 \times 10^9$ W cm^{-2} ($a = 200$) and curve (c) to $I = 10^{10}$ W cm^{-2} ($a = 330$). The integrated currents are evaluated from

$$j_{int} = \int_E^\infty j_t(E')\,\mathrm{d}E' \to \sum_{n'=n}^{\infty} j_t(n'). \tag{29}$$

The general behaviour of the data of figure 7 agrees surprisingly well with the corresponding data of figure 3 of Farkas and Tóth [8].

Since it was suggested that the observed high-energy photo-electrons have their origin in Coulomb explosion [13] due to space-charge effects, Farkas *et al* [9] performed experiments at much lower laser-field intensities, at which space-charge effects can certainly be sufficiently suppressed. Therefore we show in figure 8 our results for the transmitted and reflected currents for a moderate laser-field intensity of $I = 3.8 \times 10^6$ W cm^{-2}, in which case $a = 6.5$. In figure 8 the points correspond to the transmitted current components and the crosses to the reflected ones. These results were obtained by solving the matrix equation (25*a*) numerically. The first open channel belongs to $n = n_0 = 5$. The above-threshold peaks obtained by our model are about 30 orders of magnitude higher than those one obtains by solving the matching equations at the metal surface using Gordon–Volkov solutions or by employing time-dependent perturbation theory [10, 11]. The current distributions obtained from these latter methods could not even be drawn on a linear scale. On the other hand, our values for $j_t(n)$ are in accord with observation.

Finally we show in figure 9 data for the transmitted currents for a somewhat higher laser-field intensity of $I = 120$ MW cm^{-2}, in which case $a = 36.5$ and the matrix inversion is still possible. This case was also considered by Farkas *et al* in their experiments [9].

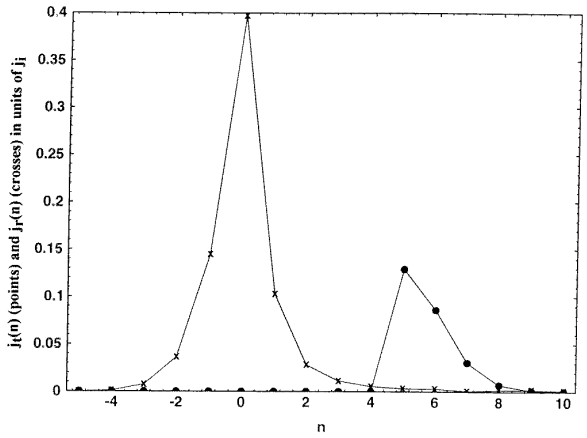

Figure 8. Shows the transmitted (points) and reflected (crosses) currents for $I = 3.8 \times 10^6$ W cm^{-2} ($a = 6.5$). The first open channel is at $n = 5$. The data were obtained by solving (21) and (22).

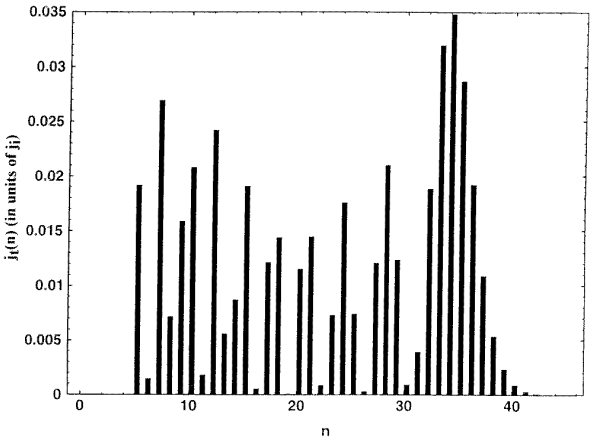

Figure 9. The transmitted currents for another somewhat higher intensity of $I = 120$ MW cm^{-2} in which case $a = 36.5$. The calculations were performed as in figure 8.

3. The generation of higher harmonics by the dipole-layer model

It is well known from harmonic generation by atoms [16] and from our earlier work on harmonic generation at metal surfaces [17] that the rates of harmonic generation can be evaluated once we know the total wavefunction of the electron which we obtained from solving the matching equations in the foregoing section. Then we only need to evaluate the expectation value of the electric dipole moment ez. Since this dipole moment will be a periodic function of time, we can expand it into a Fourier series

$$\langle e\hat{z}\rangle = \sum_n ez_n \exp(-\mathrm{i}n\omega t) \tag{30}$$

where the angle brackets indicate the quantum-mechanical average. As we know from our foregoing work, the harmonic spectra are governed by the quantity $n^3|z_n|^2$. On the basis of the wavefunction (15b) in the exterior region one can express the z_n terms in the form

$$z_n = N \sum_k \frac{T_{n+k} T_k^*}{(p_{n+k} - p_k^*)^2} \tag{31a}$$

where N is a normalization factor whose explicit value is immaterial at present. The stars mean complex conjugation, since the summation has to go over all channels, including the closed ones. We have only considered the wavefunction (15b) in the exterior region since this is the relevant part in the following analysis. Considering now the Born approximation (25c) for evaluating the transition amplitudes T_n, we can express the z_n terms of (31a) by the following analytical expression

$$z_n = N \sum_k \frac{J_{n+k}(a) J_k(-a)}{(p_{n+k} - p_k^*)^2}. \tag{31b}$$

We have numerically evaluated this sum for various values of the parameter a and calculated $n^3|z_n|^2$. We shall not, however, present any numerical data here since the approximation (31b) is much too crude, for it does not properly describe the contributions of the T_n terms for small values of n, in which case our Born approximation is invalid as shown in figures 5 and 6. Nevertheless, we can say that, according to our model, high-order harmonics should be expected for comparatively low laser-field intensities, such as those we have considered here, and that a much larger harmonic efficiency than that obtained by our elementary classical considerations in section 2 is to be expected. We only need to remind ourselves of the enormous numerical differences between the parameters a_{cl} and a. If we replace the denominator in (31b) by some constant for a crude estimate, we find on account of the addition theorem of Bessel functions that the rates of harmonic generation will be proportional to $J_n^2(2a)$ so that, on the basis of our model, very-high-order harmonics can be expected, since the spectrum will end near $n_{max} = 2a$.

4. Summary and conclusions

In the foregoing sections we have investigated a simple model of the generation of high-energy photo-electrons and high-order harmonics by shining laser light of moderate intensities of some 10^{10} W cm^{-2} at grazing incidence onto metal surfaces. This model is based on the assumption that the laser field induces at the metal surface a dipole-layer potential which is oscillating with the frequency of the laser light. Electrons of the metal are scattered by this oscillating dipole potential in the simultaneous presence of the static potential of the solid, described by the Sommerfeld step function. By means of this model we were able to explain recent observations by Farkas and co-workers [7–9] on the high-energy photo-electron spectrum without needing to resort to the mechanism of Coulomb explosion put forth as a possible explanation of these findings by Petite *et al* [13]. Moreover, we predicted by means of our model the possibility of generating high-order harmonics at metal surfaces by using comparatively low laser power, in contrast to the

results of elementary classical considerations. Our last prediction awaits experimental verification. All previous models considered to explain the above high-energy photoelectrons [10–12] have totally failed to explain the effects and their predicted probability currents of ionization were many orders of magnitude lower than the observed data would require.

Acknowledgments

This work was supported by the East–West Programme of the Austrian Academy of Sciences and by the Austrian Ministry of Science and Transportation under contract number 45.372.2-VI/6/97 and by the Hungarian National Science Foundation (OTKA) project number T016140. Moreover, we acknowledge support by the Scientific–Technical Collaboration Agreement between Austria and Hungary for 1997/98, project number A-47.

References

[1] Gavrila M 1992 *Atoms in Intense Laser Fields* (San Diego: Academic)
[2] Balcou Ph, Salières P, Budil K S, Ditmire T, Perry M D and L'Huillier A 1995 *Z. Phys D: Appl. Phys.* **34** 107
[3] Kohlweyer S, Tsakiris G D, Wahlström C-G, Tillman C and Mercer I 1995 *Opt. Commun.* **117** 431
[4] von der Linde D, Engers T, Jenke G, Agostini P, Grillon G, Nibbering E, Mysyrowicz A and Antonetti A 1995 *Phys. Rev.* A **52** R25
[5] Lichters R, Meyer-ter-Vehn J and Pukhov A 1996 *Phys. Plasmas* **3** 3425
[6] Varró S and Ehlotzky F 1996 *Phys. Rev.* A **54** 3245
[7] Farkas Gy and Tóth Cs 1989 *Fundamentals of Laser Interactions* ed F Ehlotzky (Berlin: Springer) p 289
[8] Farkas Gy and Tóth Cs 1990 *Phys. Rev.* A **41** 4123
[9] Farkas Gy, Tóth Cs and Kóházi-Kis A 1993 *Opt. Eng.* **32** 2476
[10] Daniele R, Ferrante G, Fiordilino E and Varró S 1992 *J. Opt. Soc. Am.* B **9** 1916
[11] Mishra A and Gersten J I 1991 *Phys. Rev.* B **43** 1883
[12] Martin P 1996 *J. Phys. B: At. Mol. Opt. Phys.* **29** L635
[13] Petite G, Agostini P, Trainham R, Mevel E and Martin P 1992 *Phys. Rev.* B **45** 12 210
[14] Liebsch A and Schaich W L 1989 *Phys. Rev.* B **40** 5401
[15] Ehlotzky F 1981 *Can. J. Phys.* **59** 1200
[16] L'Huillier A, Lompré L-A, Mainfrey G and Manus C [1] ch 5, p 139
[17] Varró S and Ehlotzky F 1995 *J. Phys. B: At. Mol. Opt. Phys.* **28** 121